J Nanopart Res (2014) 16:2359
DOI 10.1007/s11051-014-2359-5

RESEARCH PAPER

Exchange-biased oxide-based core–shell nanoparticles produced by seed-mediated growth in polyol

Thomas Gaudisson · Laurence Ourry · Hussein Hammoud · Sophie Nowak · Nicolas Menguy · Nader Yaacoub · Jean-Marc Grenèche · Fayna Mammeri · Souad Ammar

Received: 23 December 2013 / Accepted: 7 March 2014 / Published online: 1 April 2014

Abstract We report, for the first time, the synthesis of magnetically contrasted oxide-based core–shell nanoparticles using the polyol process. Iron oxide nanoparticles were first prepared by forced hydrolysis of iron acetate salt in a polyol and were then recovered by centrifugation and re-dispersed in a fresh cobalt acetate polyol solution. The microstructure of the resulting powder was finely characterized combining X-ray diffraction, transmission electron microscopy, and X-ray photoelectron spectroscopy. Interestingly, the produced particles appeared to be of a very high crystalline quality with a perfect epitaxy between the spinel-like iron oxide core and the rock-salt-like cobalt monoxide shell, leading to a substantial exchange bias at low temperatures. As a consequence, a net blocking temperature, T_B, increase was measured on the superparamagnetic iron oxide cores when they were coated by CoO, reaching a T_B value of 298 K, very close to room temperature.

Keywords Fe_3O_4 · Core–shell nanoparticles · Polyol process · Magnetic properties · Exchange bias

Electronic supplementary material The online version of this article (doi:10.1007/s11051-014-2359-5) contains supplementary material, which is available to authorized users.

T. Gaudisson · L. Ourry · H. Hammoud · S. Nowak · F. Mammeri · S. Ammar (✉)
ITODYS, Université Paris Diderot, Sorbonne Paris Cité, CNRS UMR-7086, Bâtiment Lavoisier, 15 Rue Jean-Antoine de Baïf, 75205 Paris Cedex 13, France
e-mail: ammarmer@univ-paris-diderot.fr

H. Hammoud · N. Yaacoub · J.-M. Grenèche
IMMM Université du Maine, LUNAM CNRS UMR-6283, Avenue Olivier Messiaen, 72085 Le Mans, France

N. Menguy
IMPMC Sorbonne Universités - UPMC Univ Paris 06, UMR CNRS 7590, MNHN, IRD, 4 Place Jussieu, 75005 Paris, France

Introduction

Magnetic exchange bias (EB) has been the focus of much attention due to its broad impact on magnetoresistive devices, non-volatile random access memories, and spintronics (Nogués and Schuller 1999; Berkowitz and Tagano 1999; Nogues et al. 2005). EB was first discovered over 50 years ago (Meiklejohn and Bean 1956, 1957), as a field shift in the hysteresis loop and enhanced coercivity (compared to that of free ferromagnetic layer), resulting from the exchange coupling between the magnetic moments located at the interface between antiferromagnetic (AF) and ferro- or ferrimagnetic (F) phases when the material is cooled in the presence of an applied magnetic field from a starting temperature between Néel temperature (T_N) and Curie temperature (T_C). Such a coupling is promoted by epitaxial interface between both magnetic phases.

Among oxide-based materials, Fe_3O_4–CoO structures have been investigated since it is already

established from physical studies that, because of the similarities in the oxygen sub-lattices of the spinel (F) and rock-salt (AF), high-quality epitaxial superlattices can be grown as thin layers by pulsed laser deposition or molecular beam epitaxy (Kleint et al. 1998; Ijiri et al. 2007). Neutron diffraction performed on such samples, namely [001] epitaxial Fe_3O_4 (10 nm)/CoO (1.7–10 nm) 50-multilayers on MgO substrates, underlined the importance of the interfacial atomic and magnetic structures in order to observe biasing mechanisms at the F/AF interface, even if the microscopic origin of EB is still not clearly understood (Ijiri et al. 1998).

Focusing on these systems, one of the most important issues of EB is the increase of the thermal stability of the Fe_3O_4 magnetization, indicated by the blocking temperature, T_B, governing the choice of the biasing materials for the design of magnetic heads. Up to now, T_B has been intensively studied as a function of AF layer thickness (D) and was found to decrease with D in epitaxial Fe_3O_4–CoO multilayers (van der Zaag 1996; Kleint et al. 1998; Ijiri et al. 1998; van der Zaag et al. 2000).

To the best of our knowledge, until now, all exchange-biased Fe_3O_4–CoO structures were produced as thin layers using physical deposition techniques, since the related routes offer the opportunity to achieve the required interfacial epitaxy and outer layer thickness control. Curiously, very few works are dealing with an extrapolation to the core–shell granular nanostructures (Pichon et al. 2013), despite their growing interest to enhance magnetic properties by coupling different magnetic phases. But now, chemists can control perfectly the previously mentioned microstructural parameters. Indeed, nanoparticles (NPs) are less expensive to produce. The nature of their F and AF components may be largely varied, and finally, they can be implemented more easily in nanodevices.

In this study, we focused on the chemical synthesis, reported for the first time, of very well-controlled core–shell $Fe_{3-x}O_4$–CoO NPs in composition, shape, and size. We used the polyol process, a versatile chemical route, for the preparation of highly crystalline, monodisperse, and isotropic in shape metal oxide nanoobjects (Basti et al. 2010; Beji et al. 2010; Artus et al. 2011). Polyols play the role of solvents, complexing ligands, and reducing agents, allowing the formation and stabilization of almost $Fe_{3-x}O_4$ and non-oxidized CoO phases, while their thermodynamical stable phases correspond to their oxidized phases γ-Fe_2O_3 and Co_3O_4, respectively. The fine microstructure of these innovative hetero-nanostructures was then investigated combining X-ray diffraction (XRD), X-ray fluorescence spectroscopy (XRF), high-resolution transmission electron microscopy (HRTEM), and X-ray photoelectron spectroscopy (XPS) while their magnetic properties were studied to evidence the core–shell structure and EB coupling.

Experimental section

Chemicals

Cobalt and iron acetate salts, as metal precursors, and diethylene glycol (DEG), as solvent, were purchased from ACROS. They were all used as-purchased, without any further purification.

Synthesis

Iron oxide NPs were prepared by forced hydrolysis in polyol medium. Generally, 23 mmol (4.0 g) of anhydrous iron acetate was dissolved in 250 mL of DEG under mechanical stirring and heated under reflux until boiling point (225 °C). NPs were then recovered by centrifugation, washed with acetone, and dried in air. 1.7 g of the recovered powder was used as seeds for cobalt monoxide growth by redispersion in a fresh DEG solution of tetrahydrate cobalt acetate (0.1 mol L^{-1}) before adding 0.9 mL of distilled water. The reaction medium was then heated up to the boiling point (180 °C) for 18 h under mechanical stirring. The cooled suspensions were centrifuged, washed with acetone, and dried in air.

Characterization

X-ray diffraction was performed on a Panalytical X'pert Pro diffractometer equipped with a multichannel detector (X'celerator) using the Co K_α radiation ($\lambda = 1.7889$ Å) in the 10–110° 2θ range (scan step of 0.025 for 2 s). Refinements were performed using MAUD program, which result from a combination of Rietveld method and Fourier analysis (Lutterotti et al. 1999). The chemical composition was checked by XRF. A drop of an aqueous suspension of the produced powder was deposited on a

clean prolene membrane and analyzed using certified solutions with appropriate Fe and Co composition on a Panalytical Epsilon 3XL spectrometer equipped with an Ag X-ray tube operating at 30 kV and 480 μA current emissions in air, during 30 s. HRTEM observations were carried out on a JEOL 2100F microscope operating at 200 kV, equipped with a field emission gun, a high-resolution UHR pole piece, and a Gatan US4000 CCD camera. The particle size distribution was estimated from the micrographs using a digital camera and the SAISAM software (Microvision Instruments), calculating the surface-average particle diameter through a statistical analysis obtained by counting about 400 particles considering a spherical particle shape. Energy Filtered TEM (EFTEM) elemental mapping was performed using the three window technique (Kundmann and Krivanek 1991). XPS spectra were recorded using a VG ESCALAB 250 system equipped with a micro-focused, monochromatic Al K_α X-ray source (1486.6 eV) and a magnetic lens. A 500-μm-sized X-ray beam was used at a power of 150 W and a potential of 15 kV. The spectra were acquired in the constant analyzer mode, with pass energy of 100 and 40 eV for the survey and the narrow regions, respectively. Charge compensation was achieved with electron flood gun. The Advantage software version 4.67 was used for data digital acquisition and processing. The peak binding energy positions were calibrated by setting the adventitious aliphatic carbon C 1s peak at 285 eV (Briggs and Seah 1990). Magnetic measurements were performed on quantum design PPMS using VSM option with a maximum applied field of 7 T in a field cooling (FC) and zero field cooling (ZFC) experimental modes. The powder was dispersed in diamagnetic alumina (4.2 wt %) and compacted into a plastic sampling tube in order to avoid grains' displacements during the measurements.

Results and discussion

Microstructural properties

X-ray fluorescence spectroscopy analysis showed that the produced powder contains cobalt and iron atoms in a Co/Fe atomic ratio of 0.78, smaller than the nominal one, namely 1.13, suggesting that only a part of cobalt salt reacted in order to form the desired cobalt oxide phase. This experimental ratio was confirmed by XRD measurements (Fig. 1).

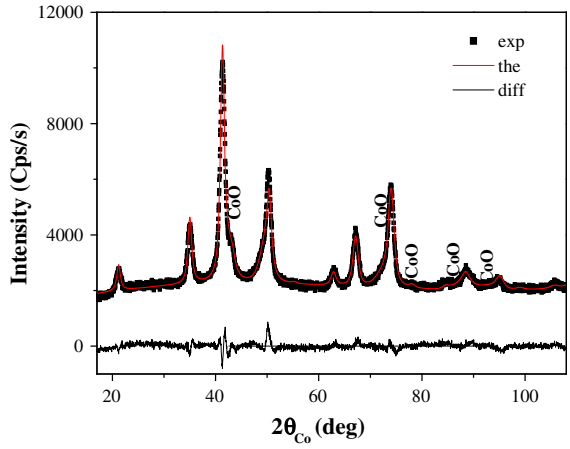

Fig. 1 The recorded (*scatters*) and calculated (*continuous line*) XRD patterns of the produced nanocomposite. The residual curve is given at the bottom of the figure for indication

The recorded XRD pattern exhibited almost broadened peaks matching very well with the spinel-like iron oxide ($Fe_{3-x}O_4$) and the rock-salt-like cobalt oxide (CoO) phases, with refined cell parameters, $a = 8.409(5)$ and 4.267(5) Å, respectively, very close to those of their bulk counterparts (ICDD n°00-019-0629 and n°00-042-1300). Considering the great probability of surface oxidation of magnetite NPs due to their reduced size, cautions have to be taken. The chemical composition of the produced iron oxide is certainly comprised between those of maghemite and magnetite phases, very probably closer to that of the latter than the former. For simplification, it will be quoted hereafter magnetite-like NPs.

Besides, the refined weight contents of the iron oxide and cobalt oxide phases, constituting the analyzed composite, were found to be about 63 and 37 wt %, respectively, with an accuracy of about 10 %, leading to an atomic Co/Fe ratio close to that determined elsewhere using XRF. Besides, MAUD analysis allowed to conclude that iron and cobalt oxides are constituted by almost strain-free and quite isotropic in shape nanocrystals of about 16 (1) and 8 (1) nm in size, respectively.

TEM experiments were performed to study the exact microstructure of the produced composite. The powder is constituted by almost isotropic (i.e., non-elongated) NPs. From high-resolution (HRTEM) observations and fast Fourier transform (FFT)

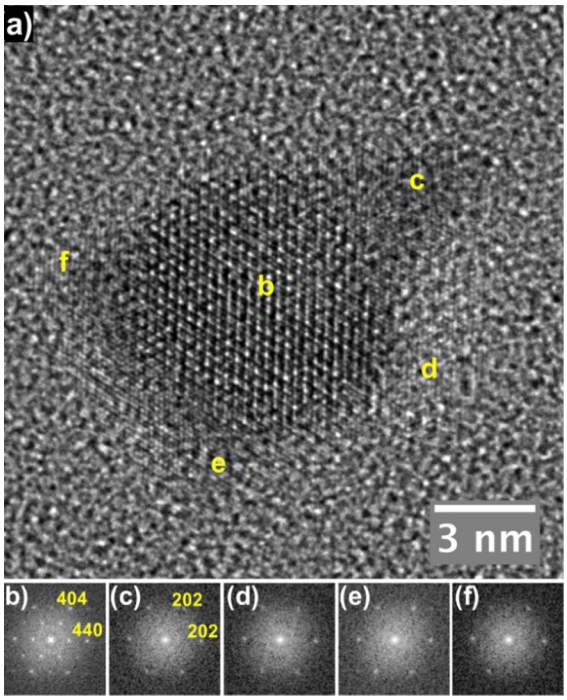

Fig. 2 **a** HRTEM image of a core–shell NP. The interfrange distance is clearly different between the central and the surrounding part of the NP. The approximate location of FFT analyses (**b**–**f**) is indicated. **b** FFT of the central area of the NP [indicated on (**a**)]. This diffraction pattern is related to a spinel structure observed along the [−111] direction. **c**–**f** FFT of the different surrounding areas indicated on (**a**). These diffraction patterns have the same orientation and correspond to CoO rock-salt observed along the [−111] direction

analyses, the structure of the NPs appears to differ between the inner core and the outer shell suggesting an almost core–shell structure (Fig. 2). This result was confirmed by EFTEM observations (Fig. 3). Indeed, the inner core corresponds to the spinel iron oxide magnetite-like with a mean size of about 10 nm, surrounded by smaller rock-salt CoO phase with a thickness smaller than 3 nm. From FFT analyses of HRTEM images, it has to be noticed that magnetite-like and CoO phases exhibit epitaxial relationships. Both phases have the same orientation within the aggregates, with no evidence of structural defects such as dislocations, stacking faults, nor surface amorphous region, establishing thus the high crystalline quality of these aggregates as textured polycrystals. This epitaxy may explain the net discrepancy between the crystal sizes inferred from XRD with those measured here by TEM. Indeed, XRD allowed measuring an average coherent domain length, labeled here $\langle L_{XRD} \rangle$, which may differ from the exact crystal size. Hence, in the case of epitaxial nanocrystals, one may a priori assume that the estimated $\langle L_{XRD} \rangle$ exceeds the real size of NPs, giving in our case lengths of about 16 nm for magnetite-like and 8 nm for CoO crystals while they appeared to be about 10- and largely less than 3-nm-sized in TEM images, respectively. Such a feature has already been observed in the case of different polyol-made spinel ferrite-textured nanocrystalline aggregates (Valenzuela et al. 2011).

Averaging the CoO crystal size on all the directions around the iron oxide core allowed us to estimate the thickness of the outer shell at approximately 1.5 nm. The respective weight ratios of each phase are estimated at about 47 and 52 wt %, respectively, from the TEM-measured magnetite-like core radius and CoO shell thickness (5.0 and 1.5 nm, respectively), assuming that the density of each phase is equal to that of the bulky state, namely 5.2 and 6.4 g cm^{-3} (Patnaik 2003), is about 47 and 52 wt %, respectively, clearly different from those estimated by XRF and XRD analyses, but surprisingly very close to the expected ones assuming a total reaction in polyol and considering the nominal cobalt- and iron-based precursors (at.-Co/Fe = 1.14 vs. 1.13). Otherwise, HRTEM observations suggested that all the magnetite-like NPs are completely coated by a continuous and almost uniform CoO shell during the seed-mediated growth process, consuming all the cobalt-based reagents, while XRD and XRF, as volume analysis techniques, suggested other scenarios: (1) a partial coverage by CoO of each Fe_3O_4 magnetite-like particle, and consequently the loss of EB feature or (2) a thinner full CoO coating of all magnetite-like particles with EB appearance. The hypothesis of a thicker complete CoO coating of only a part of the introduced magnetite-like seeds in the reaction solution was not retained. Indeed, as observed by TEM, all nano-objects are hetero-structured. Moreover, if two types of particles, free Fe_3O_4 magnetite-like and, presumably E-biased $Fe_{3-x}O_4$–CoO ones, coexist, they should answer differently to magnetic stimuli. The former are soft magnets while the latter are relatively hard ones (because of EB coupling), leading to different hysteresis contributions in the variation of the magnetization as a function of the magnetic field, at low temperature. As it will be discussed later, the recorded hysteresis loop at 5 K on the produced composite powder is found to be opened with high coercivity and remanence.

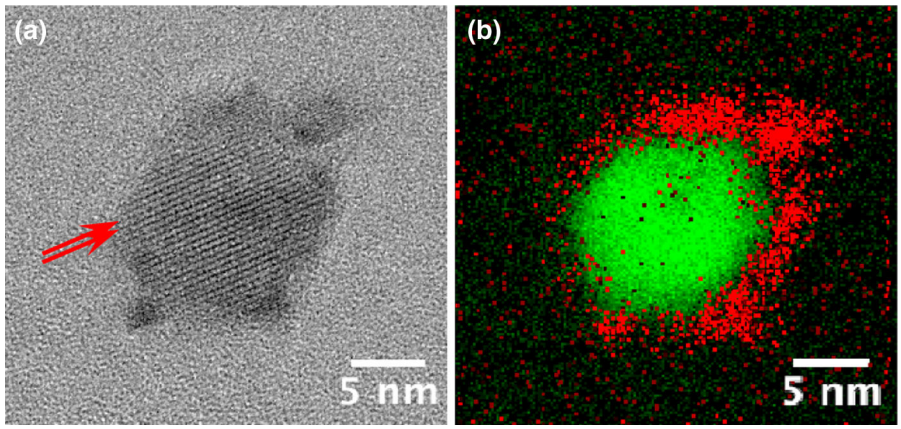

Fig. 3 EFTEM analysis of the core–shell NP. **a** Zero-loss image of a core–shell NP. The interfrange distance indicated by red arrows corresponds to d111 of the spinel structure. **b** Composite EFTEM image of the NP: *green* Co-rich phase and *red* Fe-rich phase. This composite image has been obtained using, respectively, the Co-$L_{2,3}$ and the Fe-$L_{2,3}$ edges. (Color figure online)

TEM consisted in 2D-projected image analysis. As a consequence, the TEM determined that outer shell thickness is much more a majored approximation than an exact average value, making this technique almost controversial compared to the previous ones. To tentatively conclude about the fine microstructure of the produced nanocomposite, XPS analysis was performed as a highly surface-specific technique with a typical analysis depth of 10 nm.

Fortunately, both the analysis XPS depth and the average diameter of produced NPs constituting the produced powders are of the same order of magnitude and allow us to assume XPS results as representative of the bulk composition of these NPs. XPS survey spectrum exhibits intense peaks corresponding to Fe $2p_{3/2}$, Co $2p_{3/2}$, C 1s, and O 1s at ca. 710, 783, 285, and 530 eV, respectively. The peaks at 783 and 797 eV (Fig. 4) are corresponding to the characteristic doublet related to Co and were assigned to Co $2p_{3/2}$ and Co $2p_{1/2}$, respectively; two shake-up satellite peaks at 786 and at 803 eV were observed, corresponding to Co $2p_{3/2}$ and Co $2p_{1/2}$, respectively. The presence of these two peaks and highly intense satellites was consistent with the presence of Co^{2+} cations in the high-spin state. Fe 2p high-resolution spectrum exhibited a main peak at 710 eV and a satellite at 718 eV, characteristics of the presence of Fe^{3+} cations (Fig. 4). The comparison of the intensity ratio of Fe 2p and Co 2p peaks (Fig. 4) led to the quantification of the weight ratio of each oxide phase and the estimation of the thickness of CoO outer shell.

For such a purpose, common Eq. 1 was used (Briggs and Seah 1990):

$$\frac{I(\mathrm{Co})}{I(\mathrm{Fe})} = \frac{\sigma(\mathrm{Co}) \times \mathrm{Ts}(\mathrm{Co}) \times \lambda[\mathrm{Co(CoO)}] \times C(\mathrm{Co}) \times [1 - \exp(\frac{-d(\mathrm{CoO})}{\lambda[\mathrm{Co(CoO)}] \times \cos\theta})]}{\sigma(\mathrm{Fe}) \times \mathrm{Ts}(\mathrm{Fe}) \times \lambda[\mathrm{Fe(F_3O_4)}] \times C(\mathrm{Fe}) \times \exp(\frac{-d(\mathrm{CoO})}{\lambda[\mathrm{Fe(CoO)}] \times \cos\theta})} \quad (1)$$

where σ(Fe) and σ(Co) are the photo-ionization cross section for Fe $2p_{3/2}$ and Co $2p_{3/2}$ signals, respectively; Ts(Fe) and Ts(Co) are the analyzer transmission functions of the spectrometer for each element; λ[Fe(Fe_3O_4)], λ[Fe(CoO)], and λ[Co(CoO)] are the free path of the Fe $2p_{3/2}$ or Co $2p_{3/2}$ photoelectrons in the Fe_3O_4 and CoO oxide matrices, respectively (see Supporting information); C(Fe) and C(Co) are the number of Fe and Co atoms per unit oxide volume; θ is the electron take-off angle (as a common approximation, cos θ is usually fixed to 0.5), and *d*(CoO) is the thickness of the cobalt oxide shell. Using this equation, it is possible to determine the average thickness

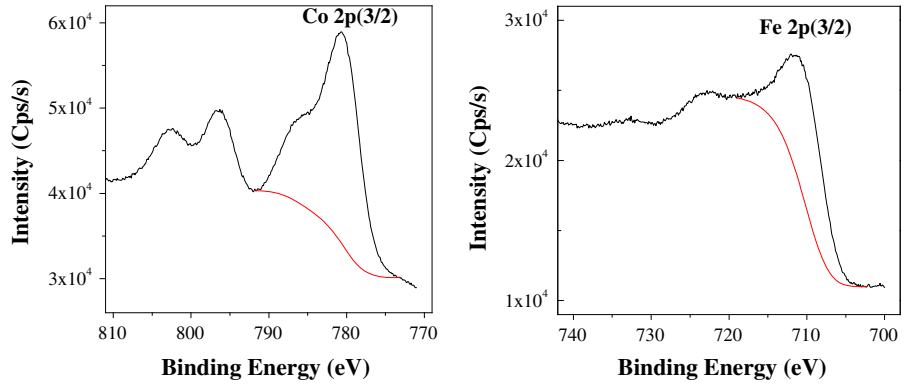

Fig. 4 High-resolution spectra of Co $2p_{3/2}$ ($E_b = 783$ eV) and Fe $2p_{3/2}$ ($E_b = 710$ eV)

of the CoO shell. It is found to be 1.7 nm with a standard deviation of ca. 20 % (mainly due to the lack of precision of the electron mean free paths). This value agrees fairly with that determined by TEM.

To modulate these results, one has to remember that the adopted model was first developed in the case of flat and thin samples. It was progressively extrapolated to granular ones, with more or less convex forms. This could be a serious limitation, since the surface irregularities may locally modify the photons' incidence angle on the analyzed substrate and then increase the crossed photon distance in the matter compared to its real thickness. In other terms, the adopted 0.5 value for cos θ parameter in the previous calculation must be used with great caution. As a consequence, the CoO layer thickness estimated from the present XPS approach is very probably overestimated. Clearly, advanced microstructural characterization of nanopowders requires combined volume and surface analysis techniques. Concerning the studied NPs, the validation of their hetero-structure requires supplementary measurements, magnetic measurements, to conclude about a total or partial CoO coating of the magnetite-like core particles.

Magnetic properties

The thermal variation of the magnetic susceptibility of bare and composite NPs was recorded in the FC and ZFC procedures under an applied magnetic field of 200 Oe (Fig. 5). All curves exhibit a net irreversibility between the FC and ZFC branches in agreement with a superparamagnetic behavior. Typically, the ZFC-$\chi(T)$ curves exhibit a cusp at a critical temperature, which usually allows the determination of the blocking temperature of the system, T_B, (Hansen and Mørup 1999; Dormann et al. 1999; Grasset et al. 2002) while the FC one remains almost constant at $T < T_B$. Comparing the two samples, an unambiguous increase of T_B was observed when iron oxide NPs were coated by CoO layer. It typically reaches ~298 K, i.e., close to room temperature, in the composite NPs, while it does not exceed ~125 K in pristine NPs. This T_B increase is attributed to EB coupling, as confirmed by the shift along the field axis of the composite hysteresis loop recorded after cooling from 300 to 5 K under an applied magnetic field of 70 kOe (Fig. 6) accompanied by a coercivity enhancement, by comparison to bare iron oxide NPs, which is another feature of EB coupling (Nogues et al. 2005). Indeed, the measured exchange and coercive field H_{EB} and H_C values using conventional formula (Trohidou et al. 2007):

$$H_C(\mathrm{FC}) = \frac{(-H_{C-} + H_{C+})}{2} \tag{6}$$

$$H_{EB}(\mathrm{FC}) = \frac{(H_{C-} + H_{C+})}{2} \tag{7}$$

where H_{c+} and H_{c-} correspond to the positive and negative values of the field for a zero magnetization, are about 142 and 500 Oe, respectively. They are much larger than those characteristics of bare NPs: 220 and 0 Oe, respectively. Altogether, these last results confirmed the existence of an interface exchange coupling between the iron oxide core and cobalt oxide shell in all the produced NPs, approving the second scenario: a total coating of the magnetite-like core by a relatively rough, thin, and continuous CoO layer.

Indeed, in the case of a non-homogeneous coating, which means a part of iron oxide cores was covered by a CoO shell while the other part was not, the measured

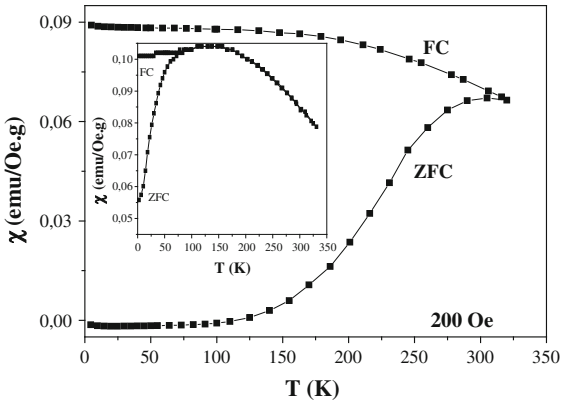

Fig. 5 Thermal variation of the magnetic susceptibility of the composite, measured in the FC and ZFC modes under an applied magnetic field of 200 Oe. In the inset that of bare iron oxide is given for indication

magnetic properties of the produced composite powder must be representative of the superposition of two kinds of superparamagnets: one assigned to iron oxide NPs with an exacerbated magnetic anisotropy due to EB (the former) and the second one to iron oxide NPs without this additional contribution (the latter). In other terms, the FC and ZFC thermal variation of the magnetic susceptibility should exhibit two irreversibilities corresponding to the values of two blocking temperatures, the highest one measured for the former NPs. Moreover, it is well established in thin films that EB properties depend strongly on the thicknesses of FM and AF layers (Nogués and Schuller 1999). In their FM–AF core–shell NP counterpart, this would be equivalent to the core diameter and the shell thickness, specifically, FM domains have to be larger than AF ones (Nogues et al. 2005). In our case, using the XRF results (CoO content of 43 wt %) and assuming a spherical particle geometry, the average thickness of the external AF shell is of about 1 nm, less widely the average diameter of the F core measured by TEM, respecting the listed above conditions.

In the case of a non-uniform coating, which means all the iron oxides seeds were coated by CoO nanocrystals which formed much more discrete dots than continuous shells around the $Fe_{3-x}O_4$ cores, EB effect should be reduced. Indeed, only a part of the AF spin structure of the CoO phase may be "frozen in" when crossing T_N, the part at the interface with the ferrimagnetic $Fe_{3-x}O_4$ phase. Accordingly, the exchange field does not reach its optimized value and can be as small as 0 Oe.

To elucidate the intimate spin structure of the interface between the two iron and cobalt oxide phases, advanced magnetic characterizations are required. Zero and in-field ^{57}Fe Mössbauer spectrometry measurements are in progress.

Conclusion

$Fe_{3-x}O_4$–CoO composite nanopowder was successfully produced by seed-mediated growth in polyol. Their fine microstructure was determined by combining XRF, XRD, TEM, XPS, and magnetometry analysis. The produced composite consisted of 10-nm-sized spherical spinel magnetite-like particles continuously coated by a rock-salt CoO shell of about 1 nm of thickness. Both phases exhibited a perfect epitaxial relationship, leading to EB coupling appearance at low temperature. As a main consequence, the blocking temperature of superparamagnetic iron oxide

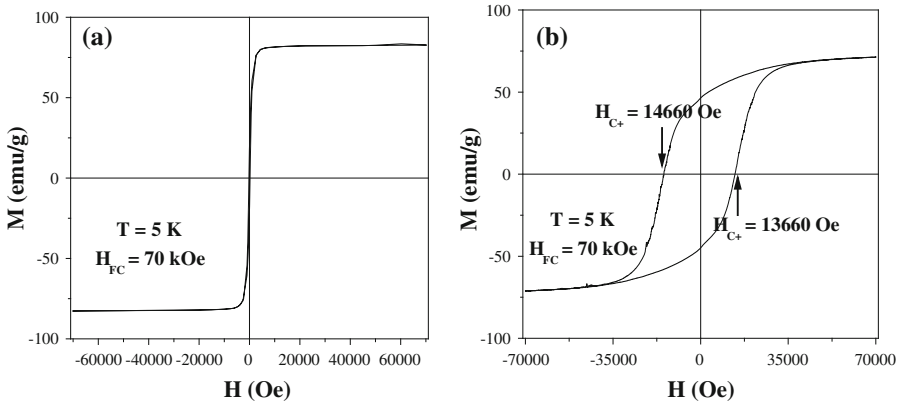

Fig. 6 *M*(*H*) curves measured in FC mode (under an applied magnetic field of 7 T) at 5 K on the as-produced bare (**a**) and composite (**b**) NPs

cores increased from 125 K (in pristine form $Fe_{3-x}O_4$) to reach 298 K (in core–shell form), under an applied magnetic field of 200 Oe, when they were coated by CoO.

Acknowledgments The authors thank Dr. Philippe Decorse (Univ. Paris Diderot) and Dr. Y. Klein (Univ. Pierre & Marie Curie) for their technical XPS and PPMS assistance and fruitful discussions. This work was supported by ANR-CONACyT research program (MINAFC).

References

Artus M, Ben Tahar L, Herbst F, Smiri LS, Villain F, Yaacoub N, Grenèche JM, Ammar S, Fiévet F (2011) Size-dependent magnetic properties of $CoFe_2O_4$ nanoparticles prepared in polyol. J Phys Condens Matter 23(50): 506001–506011

Basti H, Ben Tahar L, Smiri SL, Herbst F, Vaulay MJ, Chau F, Ammar S, Benderbous S (2010) Catechol derivatives-coated Fe_3O_4 and γ-Fe_2O_3 nanoparticles as potential MRI contrast agents. J Colloid Interface Sci 341(2):248–254

Beamson G, Briggs D (1992) High resolution monochromated X-ray photoelectron spectroscopy of organic polymers: a comparison between solid state data for organic polymers and gas phase data for small molecules. Mol Phys 76(4): 036–919

Beji Z, Smiri LS, Yaacoub N, Grenèche J-M, Menguy N, Ammar S, Fiévet F (2010) Annealing effect on the magnetic properties of polyol-made Ni–Zn ferrite nanoparticles. Chem Mater 22(4):1350–1366

Berkowitz AE, Tagano K (1999) Exchange anisotropy: a review. J Magn Magn Mater 200(1–3):552–570

Briggs D, Seah MP (1990) Practical surface analysis in Auger and X-ray photoelectron spectroscopy, vol 1. Wiley, Chichester

Dormann JL, Fiorani D, Cherkaoui R, Spinu L, Lucari F, D'Orazio F, Noguès M, Tronc E, Jolivet JP, Garcia A (1999) Collective glass state in a magnetic nanoparticle system. Nanostructured Mater 12(5–8):757–762

Grasset F, Labhsetwar N, Park DC, Saito N, Haneda H, Cador O, Roisnel T, Mornet S, Duguet E, Portier J, Etourneau J (2002) Synthesis and magnetic characterization of zinc ferrite nanoparticles with different environments: powder, colloidal solution, and zinc ferrite–silica core–shell nanoparticles. Langmuir 18(21):8209–9216

Hansen MF, Mørup S (1999) Estimation of blocking temperatures from ZFC/FC curves. J Magn Magn Mater 203(1–3):214–216

Ijiri Y, Borchers JA, Erwin RW, Lee SH, van der Zaag PJ, Wolf RM (1998) Perpendicular coupling in exchange-biased Fe_3O_4/CoO superlattices. Phys Rev Lett 80(3):608–611

Ijiri Y, Schulthess TC, Borchers JA, van der Zaag PJ, Erwin RW (2007) Link between perpendicular coupling and exchange biasing in Fe_3O_4/CoO multilayers. Phys Rev Lett 99(14):147201–147204

Kleint CA, Krause MK, Höhne R, Walter T, Semmelhack HC, Lorenz M, Esquinazi P (1998) Exchange anisotropy in epitaxial Fe_3O_4/CoO and $Fe_3O_4/Co_xFe_{3-x}O_4$ bilayers grown by pulsed laser deposition. J Appl Phys 84(9):5097–5105

Kundmann MK, Krivanek OL (1991) Automated processing of parallel-detection EELS data. Microsc Microanal Microstruct 2(2,3):245–256

Lutterotti L, Matthies S, Wenk HR (1999) MAUD: a friendly Java program for material analysis using diffraction. IUCr CPD Newsl 21:14–15

Meiklejohn WH, Bean CP (1956) New magnetic anisotropy. Phys Rev 102(5):1413–1414

Meiklejohn WH, Bean CP (1957) New magnetic anisotropy. Phys Rev 105(3):904–913

Nogués J, Schuller IK (1999) Exchange bias. J Magn Magn Mater 192(2):203–232

Nogues J, Sort J, Langlais V, Skumryev V, Surinach S, Munoz JS, Baro MD (2005) Exchange bias in nanostructure. Phys Rep 422(3):65–117

Patnaik P (2003) Handbook of inorganic chemical compounds, vol 1. McGraw-Hill, New York

Pichon P, Lefevre C, Ulhaq-Bouillet C, Grenèche J-M, Toumi M, Mhiri T, Bégin-Colin S (2013) High exchange bias in $Fe_{3-\delta}O_4$–CoO core-shell nanoparticles synthesized by a one-pot seed-mediated growth method. J Phys Chem C 117(21):11436–11443

Trohidou KN, Vasilakaki M, Del Bianco L, Fiorani D, Testa AM (2007) Exchange bias in a magnetic ordered/disordered nanoparticle system: a Monte Carlo simulation study. J Magn Magn Mater 316(2):E82–E85

Valenzuela R, Ammar S, Herbst F, Ortega-Zempoalteca R (2011) Low field microwave absorption in Ni–Zn ferrite nanoparticles in different aggregation states. Nanosci Nanotechnol Lett 3:501–598

van der Zaag JP, Ball AR, Feiner LF, Wolf RM, van der Heidjen PAA (1996) Exchange biasing in MBE grown Fe_3O_4/CoO bilayers: the antiferromagnetic layer thickness dependence. J Appl Phys 79(8):5103–5106

van der Zaag PJ, Ijiri Y, Borchers JA, Feiner LF, Wolf RW, Gaines JM, Erwin RW, Verheijen MA (2000) Difference between blocking and Néel temperatures in the exchange biased Fe_3O_4/CoO system. Phys Rev Lett 84(26): 6102–6105